Spectral separation of the efficiencies of the inside and outside orders of soft-x-ray-extreme-ultraviolet gratings at near normal incidence

Leonid I. Goray
*International Intellectual Group, Inc., P.O. Box 335, Penfield, New York 14526
and Institute for Analytical Instrumentation, Russian Academy of Sciences, Rizhsky Prospect 26,
Saint-Petersburg 190103, Russia*

John F. Seely[a)]
Space Science Division, Naval Research Laboratory, Washington, DC 20375

Sergey Yu. Sadov
*Department of Mathematics and Statistics, Memorial University of Newfoundland, St. John's,
Newfoundland A1C 5S7, Canada*

It is shown from both a phenomenological study and exact modeling that the reason for the experimentally observed substantial (a few angstroms or nanometers) separation in wavelength between the maxima of the inside (negative numbered) and outside (positive numbered) diffraction orders of a multilayer-coated grating, operating at near normal incidence and close to the Bragg condition in the soft-x-ray and extreme-ultraviolet (EUV) regions, is related to the different angles of deviation of the orders. This wavelength separation is also a feature of uncoated diffraction gratings, although not clearly noticeable. The widely used approximate approach for calculating the absolute efficiency, the product of the relative grating efficiency and the reflectance of its multilayer coating, has until recently been considered accurate enough for the analysis of soft-x-ray and EUV near-normal-incidence multilayer-coated gratings. The inapplicability of this approximation for the analysis of the precise positions and shapes of the efficiency curves for the inside and outside orders, despite the small ratios of wavelength and groove depth to period and the small angles of incidence, is demonstrated using gratings with realistic groove profiles and operating in the EUV region. The rigorous modified integral method (MIM), which is a variant of boundary integral equation methods and is designed for the calculation of the efficiency of multilayer gratings with arbitrary layer thicknesses and boundary shapes (including microroughness) and over a wide wavelength range, is proposed in a general operator formalism. An analysis of a derived simple phenomenological expression and the exact numerical study indicates that the spectral separation between the inside and the outside orders grows with increasing either wavelength, angle of incidence, groove frequency, or diffraction order number $|m|$. The efficiency modeling carried out with the commercial program PCGRATE-SX, based on the MIM, gave not only the exact values of the spectral separation between the inside and outside orders of Mo_4Ru_6/Be, Mo/Si, and Mo/Y multilayer-coated gratings with various real groove profiles measured using atomic force microscopy (AFM) but also good agreement with synchrotron radiation measurements, including high orders as well. To determine the shapes and positions of efficiency curves in the soft-x-ray-EUV range of close to normal-incidence bulk and multilayer-coated gratings with real groove profiles (measured by AFM), one should use codes based on rigorous electromagnetic theory such as the MIM. The modeling is important for developing high efficiency and dispersion gratings for high-resolution spectroscopic studies of laboratory, solar, and astrophysical radiation sources. © *2006 American Institute of Physics*. [DOI: 10.1063/1.2359224]

I. INTRODUCTION

There has been an increasing effort in the development of near-normal-incidence multilayer interference optics for soft-x-ray and extreme-ultraviolet (EUV) solar and astrophysical instruments. Multilayers were applied to various types of gratings to enhance the grating efficiency, especially for high-resolution and high dispersion spectroscopy of weak EUV sources.[1] It is now possible to reliably implement multilayer-coated diffraction gratings in spaceflight and laboratory spectrometers that operate at close to normal incidence and with high efficiency in the short-wavelength range.[2] The parameters of the multilayer coating and the groove border profiles are optimized so that the grating has high diffraction efficiency in a selected wavelength range. Methods for surface metrology,[3] such as atomic force microscopy (AFM), have advanced significantly in the last few years, driven largely by the metrology needs for advanced lithographic processes. The computational design and fabrication of the multilayer coatings also require accurate knowledge of the optical constants of layer materials.[4] An important part of the

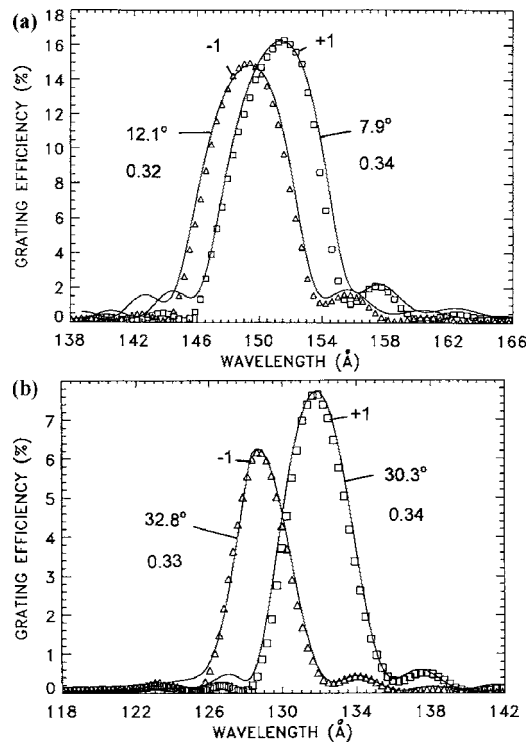a)Electronic mail: john.seely@nrl.navy.mil

FIG. 1. Measured +1 and −1 order efficiencies vs wavelength of a 2400-groove/mm multilayer-coated grating operating at angles of incidence of 10° (a) and 32° (b). The solid curves are the reflectances of the multilayer coating with 30 Mo/Si periods for the indicated angles of incidence, shifted to account for the different angles of deviation for the +1 and −1 orders. The reflectance values were reduced by factors of 0.32 and 0.34 (a) and 0.33 and 0.34 (b) which represent the groove efficiencies in +1 and −1 orders.

FIG. 2. Light diffraction on a grating working in the autocollimation (Littrow) mounting.

design process for the optimization of a grating's multilayer coating and border profiles is a computer code that accurately models the efficiency of the multilayer-coated grating.[5] The software should account for the finite conductivity of the different layers of the coating, the real shape of the borders (e.g., measured by AFM), the random microroughness and/or interdiffusion of the interfaces, and the polarization of the incident radiation.

The separation in wavelength between the inside (negative) and outside (positive) order efficiencies in a grating operating close to normal incidence in the soft-x-ray-EUV range was experimentally observed[1] in the first diffraction orders of a Mo/Si multilayer lamellar grating with 2400 grooves/mm operating at incidence angles of 10° and 32° (Fig. 1). The spectral separation of the +1 order and the −1 order efficiencies was attributed to the different angles of diffraction. This trend was confirmed in subsequent studies, including blaze gratings and higher orders.[6–8] While multilayer-coated diffraction gratings designed for operation near normal incidence in the soft-x-ray-EUV wavelength range hold the most promise, rigorous numerical modeling of their efficiency is rather time consuming.[9] Such calculations were considered over a long period of time as problematic due to weak convergence of numerical solutions and high requirements for computer memory and performance.[10] Gratings working in this wavelength range are characterized by a large number of propagating orders and the need of accounting for the effects of absorption, multiple reflection, multi-
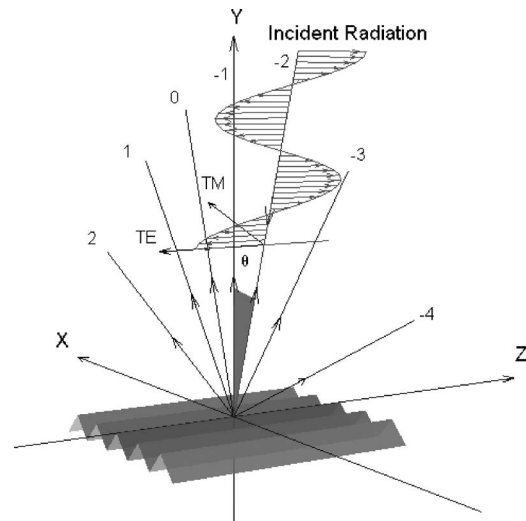
wave scattering, shadowing, and other dynamical effects that all make using the scalar or other approximate theories highly questionable.[11,12] Reliable absolute efficiency predictions for the relief gratings working in these spectral regions became possible only after the development of effective versions of the methods, the well-known differential[12,13] and integral.[5,9] References 12 and 13 presented rigorous calculations based on the differential method for gratings with ideal sawtooth border profiles with a limited number of coating layers and only for the case of the TE polarization (in the TE polarization the electric field vector is perpendicular to the plane of incidence and in the TM polarization the electric field vector lies in the plane of incidence, i.e., in the plane *XY*—see Fig. 2). The most universal and precise approach to an efficiency analysis of multilayer-coated gratings, with real groove profiles and accounting for microroughness, is a boundary integral equation method[14,15] (BIM) which makes systematic calculations in the soft-x-ray-EUV wave band feasible on a personal computer.[5,9,16]

The present paper represents a unified treatment of the calculation of the efficiencies using the same improved computational techniques and including, in particular, the effect of spectral separation of the inside and outside orders which is characteristic of various soft-x-ray-EUV gratings operating near normal incidence. Section II describes some aspects of approximate approaches of diffraction by gratings working at small wavelength-to-groove-period and wavelength-to-groove-depth ratios and their limitations. A phenomenological study of the wavelength separation of the same number |m| inside and outside orders is presented. The approximate expression derived for the separation of orders in wavelength is compared with the results obtained in rigorous numerical modeling of the efficiency of bulk, perfectly conductive lamellar gratings working under near normal incidence at low wavelength-to-period ratios. References 5, 9, 17, and 18 describe some peculiarities and implementation details of the modified integral method (MIM), which is a variant of the BIM as applied to multilayer-coated gratings working in the short-wavelength range. Section III of this paper describes

the multiboundary integral solver of the PCGRATE-S(X) code[19] in a general operator form, emphasizing details not found in the literature and important for the present study. An exact study of the efficiency of three different soft-x-ray-EUV multilayer gratings with real (AFM-measured) groove profiles, including inside and outside order separation in wavelength, is described in Sec. IV. The measurements of absolute efficiency using monochromatic synchrotron radiation are compared with calculations based on the rigorous multiboundary MIM. All modeling results covered in this paper were obtained with a commercial program PCGRATE-SX v.6.1. Section V is a summary of the paper.

II. PHENOMENOLOGICAL STUDY AND LIMITATIONS OF APPROXIMATE APPROACHES

A. Asymptotic theory predictions

A specific feature of gratings operating in the short-wavelength range is their small ratio of vacuum wavelength λ to grating period d. Despite well-known limitations, phenomenological approaches and the scalar theory of Fresnel-Kirchhoff[20] permit one to gain insight into a physical phenomenon without the costs of numerical modeling. A grating having the modulation (profile) depth h and the angles of incidence θ (measured with respect to the grating normal) and diffraction θ'_m is assumed to operate in scalar mode in order m if[21]

$$|m|\lambda/d < 0.2, \quad h/d < 0.1, \quad \theta \approx \theta'_m \sim 0°. \quad (1)$$

The scalar mode does not typically give rise to polarization effects or anomalies, and the efficiency of a perfectly reflecting grating is derived from universal curves constructed for different groove profiles. Universal curves are functions of the ratio h/d only, and they are equally applicable to gratings with different periods, groove depths, and coating materials. The Kirchhoff approximation yields for the maximum grating efficiency $E^p(m,\theta)$, which exists always for a certain ratio of Littrow wavelength to optimal groove depth h_{opt},[22]

$$E^p(\pm 1, \theta) \approx 34\% \quad \text{for a sinusoidal profile at}$$
$$\lambda_{Lit}(\pm 1)/h_{opt} \approx 3.4,$$

$$E^p(\pm 1, \theta) \approx 40\% \quad \text{for a lamellar profile at}$$
$$\lambda_{Lit}(\pm 1)/h_{opt} = 4,$$

$$E^p(m, \theta) = 100\% \quad \text{for a sawtooth profile at}$$
$$|m|\lambda_{Lit}(m)/(d \sin \delta) = 2, \quad (2)$$

where $\lambda_{Lit}(m)$ is a wavelength in autocollimation ($\theta = -\theta'_m$ for reflection and the Cartesian sign convention—see Fig. 2) and δ is a blaze angle. Due to conditions (1) the autocollimation regime is always close to normal incidence.

The simple scalar wavelength expression relating the blaze wavelength λ_B for non-Littrow mountings to the similar autocollimation wavelength is

$$\lambda_B(m) = \lambda_{Lit}(m)\cos(D_m/2), \quad (3)$$

where for the deviation angle

$$D_m = \theta + \theta'_m \quad (4)$$

the position of the maximum on the universal efficiency curve and its height vary smoothly as the grating operation deviates from the Littrow mode. Gratings with an arbitrary (for example, polygonal) groove profile are also characterized by an optimum depth, which corresponds to a maximum in the efficiency curve and is related to the coefficients of the groove profile expansion in a Fourier series.

To take into account the finite conductivity of the bulk grating material, one has only to multiply the value of the efficiency extracted from the universal curve by the Fresnel reflectance. The absolute efficiency of a soft-x-ray-EUV single-layer- or multilayer-coated grating in the mth diffraction order, $E^a_l(m,\theta)$, is represented by the product of the reflectance of a plane multilayer stack in the lth Bragg order,[23] $R_l(\theta')$, and the efficiency of a perfectly reflecting grating:[13]

$$E^a_l(m, \theta) = R_l(\theta')E^p(m, \theta), \quad (5)$$

where $\theta' = \theta$ in a general case and $\theta' = \theta - \delta$ for a sawtooth-profiled grating (the condition in which the incident ray and the diffraction order m are symmetric with respect to the working groove facet). In the case of a sawtooth profile, the rigorously calculated efficiency of a perfectly reflecting grating can be replaced by a phenomenological relation based on geometric considerations [Ref. 24, Eq. (6.3)]:

$$E^a_l(m, \theta) = R_l(\theta - \delta)\min[\cos \theta'_m/\cos \theta, \cos \theta/\cos \theta'_m]. \quad (6)$$

A fundamental constraint on the application of the approach (5) for bulk and multilayer-coated soft-x-ray-EUV gratings, as well as for gratings with one dielectric coating, is imposed by the close to normal angle of incidence, which should not be extremely grazing. For example, the incidence angle for some bulk gratings should not exceed 40°.[22] The scalar efficiency obtained from Eq. (6) was found to differ from that calculated using the rigorous differential method for a multilayer grating working at an incidence angle of 45°.[13] The critical value of the angle depends, however, on the actual grating parameters, the wavelength, the polarization, and the order number. The incidence angle at which Eqs. (5) and (6) still hold can in some cases be increased to 70°–80°.[12] As presented in Ref. 11, numerous rigorous calculations indicate that Eqs. (5) and (6) are accurate at grazing incidence only for low-frequency gratings with 300 and 600 grooves/mm. For gratings operating far from normal incidence, another approach was proposed[9] which is based on the product of the reflectance of a plane multilayer stack and the relative efficiency of a finitely conductive grating specified by one (substrate) corrugated boundary:

$$E^a_l(m, \theta) = R_l(\theta')E^a_{sub}(m, \theta)/R_{sub}(\theta'). \quad (7)$$

At the same time, numerous rigorous calculations based on the differential and integral methods demonstrated the high accuracy that Eq. (5) provides in predicting the absolute maximum efficiency in the first and higher orders of a multilayer grating with an arbitrary groove profile (including a real profile, e.g., AFM measured) and operating close to

normal incidence. Obviously, the approach (5) can be valid only for highly conformal deposited layers, a condition met primarily in the soft-x-ray-EUV range. It was believed for a long time to be a very accurate and convenient method for calculating the absolute efficiency of multilayer, near-normal-incidence gratings operating in soft-x-ray-EUV wave bands.

B. A phenomenological analysis of the orders' wavelength separation

The separation between the inside ($m < 0$) and outside ($m > 0$) diffraction orders in wavelength for a grating with an arbitrary groove profile shape can be estimated from Eq. (4) for any order. We find θ'_m from the grating equation

$$\sin \theta - \sin \theta'_m = -m\lambda/d \tag{8}$$

taking into account the smallness of the angles of incidence and diffraction and substitute this expansion into Eq. (4):

$$D_m \approx 2\theta + m\lambda/d. \tag{9}$$

Next we write the difference $\Delta\lambda_B$ between the spectral positions of the maxima in the $-|m|$ and $+|m|$ orders in the form

$$\begin{aligned}\Delta\lambda_B &= \lambda_B(-|m|) - \lambda_B(+|m|)\\ &= \lambda_{\text{Lit}}[\cos(D_{-|m|}/2) - \cos(D_{+|m|}/2)].\end{aligned} \tag{10}$$

It can be shown by algebra and accounting for the smallness of the angles of incidence and diffraction that

$$\Delta\lambda_B \approx |m|(\lambda_{\text{Lit}}\theta)(\lambda/d). \tag{11}$$

Equation (11) shows that the spectral separation of the same number inside and outside orders grows with increasing order number, wavelength, angle of incidence, and grating frequency. Strictly normal incidence does not give rise to order separation in wavelength.

C. Comparison between phenomenological and numerical results of spectral orders' separation for bulk gratings

Compare now the values of $\Delta\lambda_B$ obtained with the approximate relation (11) with the results of rigorous numerical modeling. As an illustration, consider gratings with perfect conductivity and a symmetric lamellar groove profile working in the TE-polarized soft-x-ray-EUV radiation (the polarization difference between efficiencies is negligible for such gratings).

Figure 3 displays the spectral response curves of efficiency in the ±1 and ±5 orders obtained for a 2400-groove/mm lamellar grating with 2.5-nm-deep grooves and 0.5 land-to-period ratio. The maximum efficiencies in the −1 order lie at a wavelength of approximately 9.8 nm for an angle of incidence of 10° and at a wavelength of approximately 8.7 nm for an angle of incidence of 30° [Fig. 3(a)]. As seen from Figs. 3(a) and 3(b), the wavelength separation between the efficiency maxima of the inside and outside orders of the same number increases with increasing order number and angle of incidence, which is consistent with Eq. (11). The wavelength separations $\Delta\lambda_B$ obtained from Eq. (11) for the first diffraction order are 0.4 Å for $\theta = 10°$ and
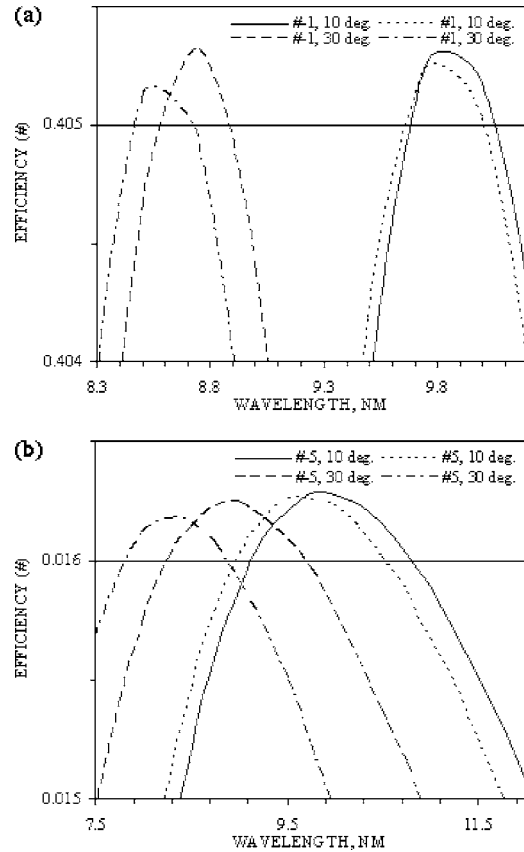

FIG. 3. Rigorously calculated ±1 (a) and ±5 (b) order efficiencies vs wavelength of perfectly conductive 2400-groove/mm lamellar gratings with 2.5-nm-deep grooves and 0.5 land-to-period ratio operating at angles of incidence of 10° and 30°.

1.1 Å for $\theta = 30°$. As seen in Fig. 3, all values are in good quantitative agreement with the separation between the indicated inside and outside orders derived by rigorous calculations despite the fairly large angles of incidence. This is accounted for by the small values of h_{opt} and, respectively, λ_{Lit} for which Eq. (11) is met with a high accuracy.

Figure 4 presents curves of efficiency in the ±1 and ±3 orders obtained for 1200- and 2400-groove/mm lamellar gratings with 5-nm-deep grooves and 0.5 land-to-period ratio at an angle of incidence of 30°. The corresponding first-order peak efficiencies lie at a wavelength of ∼17.3 nm [Fig. 4(a)]. As seen in Figs. 4(a) and 4(b), the wavelength separation between the efficiency maxima of the inside and outside orders of the same number increases with increasing order number and decreases with increasing groove spacing in accordance with Eq. (11). The wavelength separation $\Delta\lambda_B$ obtained from Eq. (11) for the first diffraction order of the 1200-groove/mm grating is 2.2 Å and for the 2400-groove/mm grating is 4.3 Å. As seen in Fig. 4, the $\Delta\lambda_B$ values obtained using Eq. (11) are about one half the actual separations between the corresponding plus and minus order efficiencies yielded by rigorous calculations. This should be primarily attributed to the large angle of incidence, for which Eq. (11) is no longer accurate.

A comparison of the examples described in Figs. 3 and 4 for the angle of incidence of 10° (not shown) indicates that the spectral separation between the same number inside and
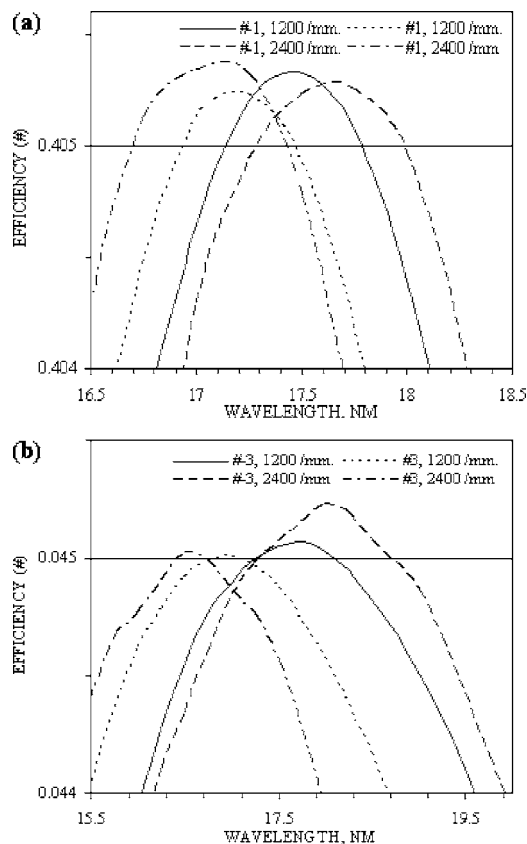
FIG. 4. Rigorously calcualted ±1 (a) and ±3 (b) order efficiencies vs wavelength of perfectly conductive 1200 and 2400-groove/mm lamellar gratings with 5-nm-deep grooves and 0.5 land-to-period ratio operating at an angle of incidence of 30°.

outside orders grows approximately fourfold when the wavelength increases by a factor 2, which likewise is in good accord with Eq. (11).

The analysis outlined in this section and in Sec. II B suggests that the wavelength separation of the inside and outside order efficiencies is related to oblique, close to normal incidence of light on a grating operating in the short-wavelength spectral region and to different angles of deviation for these orders. The spectral separation of the inside and outside orders with equal order number is fitted well by the approximate relation (11) for small values of the parameters in parentheses on its right-hand side. This separation is, however, fairly small in absolute magnitude and, in view of the slowly varying efficiency curves of different orders obtained for bulk gratings, is of no particular significance for this type of grating. By contrast, for multilayer-coated gratings whose efficiency maxima are determined by the Bragg reflection peaks, the wavelength separation between the inside and outside orders is reliably observable in various experiments and is significant. To quantitatively study this effect as applied to multilayer gratings, one could modify Eqs. (5)–(7) to correct the angle of incidence θ'' in order to calculate the reflectance of a multilayer-coated mirror with due account of the wavelength separation between the same number positive and negative orders. For example, one could replace θ' by the diffraction angle θ''_m as was done in Ref. 1 [Fig. 9(a)], by the angle of deviation D_m, or by taking the

geometric mean of the reflectances of multilayer coatings calculated for the angles of incidence and diffraction.[25] Because of the approximate nature of this approach inherent in the physical model involved, it can yield a reasonable result in one case which would fit an experiment while proving erroneous in another.[12] Since the exact outcome is not known in advance, one should always perform a comparison with experiment or with rigorous calculations.

III. DYNAMICAL THEORY FOR MULTILAYER GRATINGS

A. Physical and mathematical models in calculating multilayer grating efficiency

The efficiency calculations of multilayer-coated gratings performed in the earlier studies[1,6–8] made use of a model based on Eq. (5) or its refined version (7). The latter takes into account the finite conductivity of the substrate and yields realistic results for both normal and grazing angles of incidence. While theoretical calculations based on the approximate physical models (5) and (7) predict quite well the peak height of the efficiency curves in different orders, they do not yield the efficiency curve shapes and the noticeable spectral separation of the inside and outside orders observed in experiments.

A numerical analysis of the experimentally observed spectral separation between the inside and outside order efficiencies of a multilayer grating with a real groove profile was carried out[4] by invoking the rigorous MIM method (Ref. 17) generalized on the multiboundary scheme of integral equations.[18] The exact modeling was performed by use of the PCGRATE-SX program[19] and not only permitted theoretical validation of the spectral separation between the inside and outside orders of a multilayer 2400-groove/mm Mo$_4$Ru$_6$/Be grating with a real (AFM-measured) blazed groove profile but also provided good agreement with experimental results covering a wide wavelength range and including higher orders as well. The recently calculated wavelength separation between the inside and outside order efficiencies of a multilayer Mo/Si 4200-groove/mm grating with a real trapezoidal groove profile, which was designed for operation in the EIS spectrometer on the Solar-B spacecraft, was in good agreement with the synchrotron radiation measurements[23] in two EUV wavelength regions. Precise efficiency calculations of a 2400-groove/mm Mo/Y grating with a real groove profile operating at 8° incidence in the 9 nm wavelength range were also reported[26] and included the observed significant separation between the inside and outside order efficiencies.

The PCGRATE-S(X) code, based on the BIM, is used in the present work to analyze the diffractive properties of single-layer and multilayer gratings with arbitrary angles of incidence, boundary shapes, and layer thicknesses, including nonconformal layers and real-profile boundaries. The multiboundary solver implemented in PCGRATE-S(X) is based on the algorithm first described in Ref. 14. A more transparent and detailed exposition, including a discussion of various marching schemes that avoid hypersingular potential operators, is given in Ref. 15. The scheme in our program is the
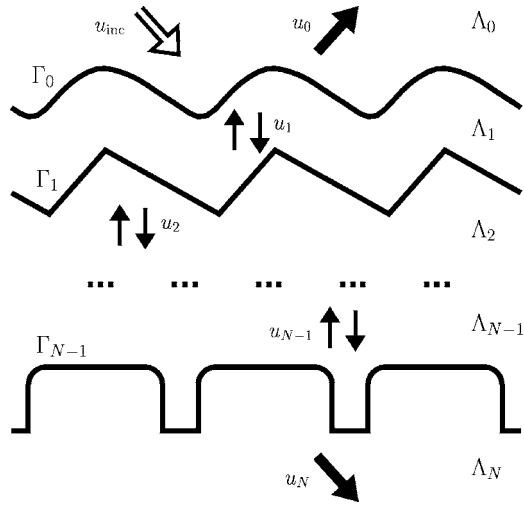
FIG. 5. Schematic of a slab grating.

original one of Maystre, Variant D in each layer by Pomp's classification (Ref. 15, p. 113).

Analytical aspects of boundary integral operators are well described in the literature; see, for example, Ref. 15 or Ref. 27. They are not touched upon here except in a few remarks. In addition, some details of the PCGRATE code, including the discretization and particular algorithmic enhancements for small λ/d ratios, are described elsewhere.[17,18] By contrast, the upper-level structure of the multilayer algorithm is not sufficiently emphasized in the existing publications. In order to make the algorithm more accessible and general, we explicitly write out a chain of operator equations, omitting details not pertinent to the structural level.

Consider a multilayer structure consisting of $N+1$ homogeneous material layers $\Lambda_0, \ldots, \Lambda_N$, characterized by their refractive index $\nu_j = (\varepsilon_j \mu_j)^{1/2}$, $j = 0, \ldots, N$, and N periodic interfaces $\tilde{\Gamma}_0, \ldots, \tilde{\Gamma}_{N-1}$ (Fig. 5), where ε_j are electric permittivities and μ_j are magnetic permeabilities. A fixed part of each interface $\tilde{\Gamma}_j$ embracing exactly one grating period will be denoted Γ_j. [We prefer the enumeration beginning with 0 for two reasons. First, the material layer number 0 is often air (or vacuum), so it is not part of a fabricated grating. Second, this enumeration is directly compatible with array indexing in C++, which is the language of choice for the software discussed.]

We refer to the semi-infinite layer Λ_0 as the top layer and to Λ_N as the bottom layer. It is assumed that the light is incident from Λ_0. The bottom layer is semi-infinite downward. We formally include the bottom layer into consideration even if the lowest medium is a perfect conductor, in which case Λ_N is ignored in the computational procedure.

For every $j = 0, \ldots, N-1$, the lower boundary of the layer Λ_j is $\tilde{\Gamma}_j$, which will be called the floor of the layer Λ_j. Similarly, for each $j = 0, \ldots, N-1$, we call the upper boundary $\tilde{\Gamma}_{j-1}$ of the layer Λ_j the ceiling of Λ_j.

Note that we allow the y projections of the boundaries to be overlapping. This is vital in the modeling of coated gratings.

B. Fields and boundary conditions

In this paper we are concerned with pure TE and TM polarizations and nonmagnetic media ($\mu_j = 1$). The fields are assumed time harmonic. Under these conditions, the Maxwell system of equations reduces to a single Helmholtz equation; therefore fields are represented in the sequel by scalar functions. They would be two-component vector functions in the case of conical (off-plane) diffraction, which will be discussed in detail elsewhere. The total field in Λ_0 is the sum of the incident field $u_{inc}(x, y)$ and the reflected field $u_0(x, y)$ and in Λ_N only the transmitted field $u_N(x, y)$ is present. For $j \geq 1$, the induced field inside the layer Λ_j is denoted $u_j(x, y)$. The solver only deals with boundary values of the fields and their normal derivatives. For a scalar function $u(x, y)$ defined near Γ_j (from either side), we take the normal derivative $\partial_n u = n_x \partial_x u + n_y \partial_y u$ directed inward Λ_j, that is upward for Γ_j described explicitly as $y = f(x)$. In general, the boundary Γ_j can be described by parametric equations $x = x(t)$, $y = y(t)$ with parameter t. We deem that Λ_j lies to the left from Γ_j as t increases. Then the components of the normal vector to Γ_j are $n_x = y'(x'^2 + y'^2)^{-1/2}$, $n_y = x'(x'^2 + y'^2)^{-1/2}$, where the prime denotes d/dt.

For $j = 0, \ldots, N-1$ define the functions on the boundaries:

$$u_j^+ = u_j|_{\Gamma_{j-1}}, \quad v_j^+ = \left.\frac{\partial u_j}{\partial n}\right|_{\Gamma_{j-1}},$$

$$u_j^- = u_j|_{\Gamma_j}, \quad v_j^- = \left.\frac{\partial u_j}{\partial n}\right|_{\Gamma_j}. \tag{12}$$

Thus there are four values attributed to every boundary Γ_j: the upper values u_j^-, v_j^- (that belong to the layer Λ_j and are the floor values for that layer) and the lower values u_j^+, v_j^+ (that belong to the layer Λ_{j+1} and are the ceiling values for that layer). These four values obey the standard boundary conditions of Maxwell's theory.

If Γ_j is a penetrable interface (separating dielectric or finitely conducting layers) then

$$u_j^- + \delta_{j0} u_{inc} = u_{j+1}^+, \quad v_j^- + \delta_{j0} v_{inc} = \kappa_j v_{j+1}^+. \tag{13}$$

Here δ_{j0} is the Kronecker symbol, $v_{inc} = \partial_n u_{inc}$ and

$$\kappa_j = \begin{cases} 1 & \text{for TE polarization} \\ (\nu_j/\nu_{j+1})^2 = \varepsilon_j/\varepsilon_{j+1} & \text{for TM polarization.} \end{cases} \tag{14}$$

Only one boundary condition is required if the lower layer Λ_{j+1} is perfectly conducting (and hence necessarily $j+1 = N$):

$$u_j^- = 0 \quad \text{for TE polarization,}$$

$$v_j^- = 0 \quad \text{for TM polarization.} \tag{15}$$

In addition, in the homogeneous regions Λ_j, $j = 0, \ldots, N$ (excluding boundaries Γ_j, $j = 0, \ldots, N-1$) the field u_j satisfies the homogeneous scalar Helmholtz equation:

$$\Delta u_j + k_j^2 u_j = 0, \tag{16}$$

where $k_j = k_0(\nu_j/\nu_0) = 2\pi(\nu_j/\nu_0)/\lambda$ is the wave number in medium number j. Denote, as usual [see, e.g., Ref. 24, Eq. (1.42)]
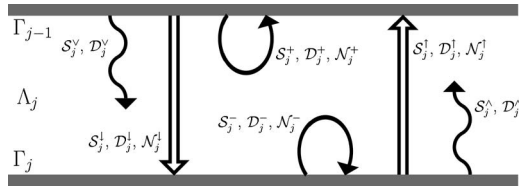
FIG. 6. Potential operators in a single grating layer.

$$\alpha_m = k_0 \cos\theta + 2\pi m/d, \quad m = \pm 0, \pm 1, \pm 2, \ldots,$$

$$\beta_m{}^{(j)} = (k_j^2 - \alpha_m^2)^{1/2}, \tag{17}$$

and the square root branch is such that $\mathrm{Re}(\sqrt{\ }) \geq 0$ and $\mathrm{Im}(\sqrt{\ }) \geq 0$. The reflected field is given by the Rayleigh expansion which in the far zone reduces to a finite sum of propagating plane waves with reflected order amplitudes $c_m{}^+$: for (x,y) in Λ_0

$$u_{\mathrm{refl}}(x,y) = \sum_{|\alpha_m| < k_a} c_m{}^+ \exp(i\alpha_m x + i\beta_m^{(0)} y)$$

$$+ \text{ evanescent waves.} \tag{18}$$

The reflection coefficient is defined as

$$R = \sum_{|\alpha_m| < k_0} |c_m{}^+|^2 \frac{\beta_m^{(0)}}{\beta_0^{(0)}}. \tag{19}$$

Summands in R are called reflected order efficiencies. If the lower medium is a lossless dielectric [$\mathrm{Im}(k_N)=0$] (case of transmission grating), then we define the Rayleigh coefficients c_m^- of the transmitted field [for (x,y) in Λ_N]

$$u_{\mathrm{transm}}(x,y) = \sum_{|\alpha_m| < k_N} c_m{}^- \exp(i\alpha_m x - i\beta_m^{(N)} y)$$

$$+ \text{ evanescent waves} \tag{20}$$

and the transmission coefficient

$$T = \left(\frac{\kappa_N}{\kappa_0}\right)^2 \sum_{|\alpha_m| < k_N} |c_m{}^-|^2 \frac{\beta_m^{(N)}}{\beta_0^{(0)}}. \tag{21}$$

Similar to (19), summands in T are called transmitted order efficiencies.

C. Potentials

Relations between boundary values of the fields across the layers can be found in terms of boundary potentials. Let us introduce potential operators using the following notational conventions (see Fig. 6). If $P=\mathrm{SL}$ or $P=\mathrm{DL}$ is the family name of operators of single-layer or double-layer potentials, we have the following.

(a) $P_j{}^\vee$ denotes the operator that takes a single variable function on the ceiling Γ_{j-1} of the layer Λ_j and produces a function of two variables in Λ_j.

(b) $P_j{}^\wedge$ denotes the operator that takes a single variable function on the floor Γ_j of the layer Λ_j and produces a function of two variables in Λ_j.

(c) $P_j{}^\downarrow$ denotes the operator that takes a single variable function on the ceiling Γ_{j-1} of the layer Λ_j and pro-

duces a function of two variables on the floor Γ_j of the same layer. Thus $P_j{}^\downarrow$ is $P_j{}^\vee$ composed with restriction onto the boundary Γ_j.

(d) $P_j{}^\uparrow$ denotes the operator that takes a single variable function on the floor Γ_j of the layer Λ_j and produces a function of two variables on the ceiling Γ_{j-1} of the same layer. Thus $P_j{}^\uparrow$ is $P_j{}^\wedge$ composed with restriction onto the boundary Γ_{j-1}.

(e) $P_j{}^\pm$ denote the singular boundary potential operators on the upper and lower boundaries of Λ_j, respectively. If φ is a function on Γ_j, then $\psi = P_j{}^-[\varphi]$ is also a function on Γ_j defined as the nontangent limit

$$\psi(x_*, y_*) = \lim_{\Lambda_j \ni (x,y) \to (x_*, y_*)} P_j{}^\wedge[\varphi](x,y), \quad (x_*, y_*) \in \Gamma_j. \tag{22}$$

Finally, define families of operators that involve normal derivatives on the boundaries. There are two such families, namely, normal derivatives of single- and double-layer potentials (NSL and NDL). Similar to the above, where P means either SL or DL, we now write NP meaning either NSL or NDL. The operators $NP_j{}^\downarrow$ and $NP_j{}^+$ take a function φ on the ceiling Γ_{j-1} of Λ_j and produce the normal derivatives of the potential $P_j{}^\vee[\varphi]$ on Γ_j and Γ_{j-1}, respectively. Similarly, the operators $NP_j{}^\uparrow$ and $NP_j{}^-$ take a function on Γ_j to functions on Γ_{j-1} and Γ_j equal to the normal derivatives of the potential defined through $P_j{}^\wedge$.

Remark. There are no operators of the form $P_0{}^\uparrow$, $P_0{}^\downarrow$, $P_N{}^\uparrow$, $P_N{}^\downarrow$, $P_0{}^+$, $P_N{}^-$, where the notation refers to nonexistent boundaries of the semi-infinite layers Λ_0, Λ_N.

The operators $P^\uparrow$, $P^\downarrow$, $NP^\uparrow$, and $NP^\downarrow$, connecting values on different boundaries, are nonsingular. The operators $P^\pm$ and $NP^\pm$ that take a function to a function on the same boundary are singular. Recall that P stands for SL or DL. We use the families SL, NSL, and DL of boundary operators. The two-character notation can cause some inconvenience in equations containing products of operators. For this reason, we use the following single-letter abbreviations:

$$S = \mathrm{SL}, \quad \mathcal{N} = \mathrm{NSL}, \quad D = \mathrm{DL}, \tag{23}$$

The family NDL containing hypersingular boundary operators is not currently used in our program; therefore we do not introduce a single-letter abbreviation for it. Including it in a solver would bring a flexibility sufficient to avoid poor conditioning due to internal eigenvalues.[28] [In practice the eigenvalues seldom cause problems, even in large series of computations performed in an automatic scanning regime with varying parameter(s).]

Detailed discussion, formulas, and jump relations for potential operators can be found in many sources. Table I shows the correspondence between our notation and that in Ref. 15. In the first ten rows, we refer to p. 111 in Ref. 15, and our layers Λ_j, Λ_{j+1} correspond to Pomp's M_u, M_L, respectively. In the last six rows, we refer to p. 114 in Ref. 15.

The value of the field at any location can be found from the boundary data by using Green's formula. Inside the inner layer Λ_j, we have

TABLE I. Correspondence between operator notations in two papers

This paper	Ref. 15
$S_j^\wedge$	G_+
$S_{j+1}^\wedge$	G_-
$D_j^\wedge$	N_+
$D_{j+1}^\vee$	N_-
S_j^+	$V_+ G_+$
S_{j+1}^-	$V_- G_-$
$\mathcal{N}_j^+$	$U_+ G_+$
$\mathcal{N}_{j+1}^-$	$U_- G_-$
D_j^+	$V_+ N_+$
D_{j+1}^-	$V_- N_-$
$S_j^\uparrow$	$V_-{}^\Theta G_2{}^\Gamma$
$S_j^\downarrow$	$V_+{}^\Gamma G_2{}^\Theta$
$\mathcal{N}_j^\uparrow$	$U_-{}^\Theta G_2{}^\Gamma$
$\mathcal{N}_j^\downarrow$	$U_+{}^\Gamma G_2{}^\Theta$
$D_j^\uparrow$	$V_-{}^\Theta N_2{}^\Gamma$
$D_j^\downarrow$	$V_+{}^\Gamma N_2{}^\Theta$

$$u_j = S_j^\wedge[v_j^-] - D_j^\wedge[u_j^-] - S_j^\vee[v_j^+] + D_j^\vee[u_j^+]. \tag{24}$$

(Evaluation of the potentials near boundaries involves singular integration and requires special numerical techniques.[29,30]) Formulas for the diffracted field in Λ_0 and Λ_N contain only two terms. Diffraction efficiencies or far field patterns for the reflected and transmitted fields can easily be found from the corresponding boundary values. Collecting the reflection and transmission coefficients, which are the summands in Eqs. (19) and (21) into vectors **r** and **t**, one can express them in a compact form as

$$\mathbf{r} = S_0^{+\infty}[v_0^-] - D_0^{+\infty}[u_0^-],$$

$$\mathbf{t} = D_N^{-\infty}[u_N^+] - S_N^{-\infty}[v_N^+], \tag{25}$$

with appropriate vector-valued functionals [Ref. 27, Eq. (26)] applied to the boundary functions. For lossy gratings, also the absorption coefficient can be calculated as a boundary integral from u_0^-, v_0^-, u_N^+, v_N^+.[18]

We note a certain freedom in the choice of the potential operators, more specifically, of Green's functions (kernel functions). First, Green's functions in the operators P_0 and P_N must be outgoing upward and downward respectively. This is dictated by the radiation conditions satisfied by the reflected and transmitted fields. It is not mathematically necessary that Green's functions in the inner layers possess such directional propagation properties, though it is customary to have downward propagating kernels in the $P^\vee$ (and induced) operators and upward propagating kernels in the $P^\wedge$ (and induced) operators. Second, Green's function in an inner layer is defined up to addition of an arbitrary solution of the homogeneous Helmholtz equation. In particular, an arbitrary finite linear combination of typical plane waves can be added to Green's function. It seems that opportunities offered by this observation for improving the efficiency of Green's function computations have not been explored.

D. Marching procedure

Green's formula representation of the field (24) can be used to obtain a chain of integral equations from which the boundary functions u_j, v_j can be found. However, in that approach normal derivatives of double-layer potentials would arise. Maystre's scheme avoids this technical complication. Instead of Eq. (24), an alternative representation of the field is exploited:

$$u_j = S_j^\wedge[v_j^-] - D_j^\wedge[u_j^-] + S_j^\vee[\varphi_j]. \tag{26}$$

The functions φ_j are unknown densities of single-layer potentials defined on the layer ceilings. For the bottom layer set

$$u_{N+1} = S_{N+1}^\vee[\varphi_{N+1}]. \tag{27}$$

Suppose that the ceiling functions of the layer Λ_{j+1} are expressed in terms of the density φ_{j+1} in the operator form

$$\begin{bmatrix} u_{j+1}^+ \\ v_{j+1}^+ \end{bmatrix} = \begin{bmatrix} Y_{j+1} \\ Z_{j+1} \end{bmatrix} [\varphi_{j+1}]. \tag{28}$$

Let us find a similar expression for the layer Λ_j and derive a backward recurrence for the operators Y and Z. Let $j > 0$. Using the boundary conditions (13), we get

$$u_j^- = Y_{j+1}\varphi_{j+1}, \quad v_j^- = \kappa_j Z_{j+1}\varphi_{j+1}. \tag{29}$$

On the other hand, the representation (26) implies

$$u_j^- = S_j^-[v_j^-] - D_j^-[u_j^-] + S_j^\downarrow[\varphi_j]. \tag{30}$$

Substituting (29) to (30) and solving for φ_{j+1}, we obtain

$$\varphi_{j+1} = Q_j[\varphi_j], \tag{31}$$

where the transfer operator Q_j is the solution of the operator equation

$$[(I + D_j^-)Y_{j+1} - S_j^- \kappa_j Z_{j+1}]Q_j = S_j^\downarrow, \tag{32}$$

where I is the identity operator which takes any function on Γ_{j+1} into itself. It follows from (26) and (29) that

$$u_j^+ = (S_j^\uparrow \kappa_j Z_{j+1} - D_j^\uparrow Y_{j+1})[\varphi_{j+1}] + S_j^+[\varphi_j]; \tag{33}$$

therefore comparing with (28) we obtain

$$Y_j = (S_j^\uparrow \kappa_j Z_{j+1} - D_j^\uparrow Y_{j+1})Q_j + S_j^+. \tag{34}$$

To obtain a formula for Z_j, let the observation point in Green's formula (24) be on Γ_j. The formula becomes

$$u_j^+ = S_j^\uparrow[v_j^-] - D_j^\uparrow[u_j^-] - S_j^+[v_j^+] + D_j^+[u_j^+]. \tag{35}$$

On the other hand, by (26),

$$u_j^+ = S_j^\uparrow[v_j^-] - D_j^\uparrow[u_j^-] + S_j^+[\varphi_j]. \tag{36}$$

Subtraction yields

$$S_j^+[v_j^+] - D_j^+[u_j^+] + S_j^+[\varphi_j] = 0. \tag{37}$$

Compare this with (28), where $j+1$ is replaced by j, and obtain

$$Z_j = (S_j^+)^{-1}(-S_j^+) + D_j^+(Y_j). \tag{38}$$

The formulas (32), (34), and (38) constitute the down-up marching procedure. It remains to specify the initial values

Y_{N+1} and Z_{N+1}. In the case of an infinitely conducting bottom layer, one can set

$$\begin{bmatrix} Y_{N+1} \\ Z_{N+1} \end{bmatrix} = \begin{bmatrix} 0 \\ I \end{bmatrix} \quad \text{for TE,} \quad \begin{bmatrix} Y_{N+1} \\ Z_{N+1} \end{bmatrix} = \begin{bmatrix} I \\ 0 \end{bmatrix} \quad \text{for TM.} \tag{39}$$

Otherwise, according to (27), set

$$Y_{N+1} = S^+_{N+1}. \tag{40}$$

The operator Z_{N+1} is then found by the general formula (38).

Equation for the top layer. The layer Λ_0 needs special treatment, but the equations are similar. In Eq. (28) with $j = 0$, the third term is absent. The boundary condition (13) includes the incident wave. Instead of Eq. (32), we obtain

$$\{(I + D_0^-)Y_1 - S_0\kappa_0 Z_1\}\varphi_1 = (I + D_0^-)u_{\text{inc}} - S_0^- v_{\text{inc}}. \tag{41}$$

The function φ_1 is found from Eq. (30). Then $\varphi_2, \ldots, \varphi_{N+1}$ are found recurrently by Eq. (31). If the bottom layer is perfectly conducting, the recurrence terminates at φ_N.

Assuming that the potential operators are available now as ready-to-use building blocks, an object-oriented implementation of the operator equations becomes relatively easy. Such implementation allows one to treat exactly complex grating structures with hundreds of boundaries having real profiles with a fine structure (microroughness) at very low λ/d ratios ($< 1 \times 10^{-4}$) on a personal computer. Three concrete examples of efficiency modeling, performed with a computer program based on the outlined scheme, and comparisons to synchrotron radiation measurements are presented below in a common format. The comparative study includes the orders' wavelength separation for different kinds of soft-x-ray-EUV gratings.

IV. SAMPLES OF SEPARATION IN WAVELENGTH OF INSIDE AND OUTSIDE ORDER EFFICIENCIES OF MULTILAYER-COATED GRATINGS

A. Investigation of the efficiency of a blazed MoRu/Be grating

The use of Be as the transmissive spacer material permits the operation of gratings at wavelengths as short as the beryllium K absorption edge at 11.07 nm. The efficiencies of the multilayer gratings, greatly enhanced by the MoRu/Be coatings, were measured using synchrotron radiation in the 11.1–12.0 nm wavelength range.[7] The multilayer gratings were produced by applying Mo_4Ru_6/Be multilayer coatings to replicas of a concave ion-etched holographic master grating with 2400 grooves/mm and a 2 m radius of curvature. The replica grating pattern covered an area of 45×35 mm^2.[5] The Mo_4Ru_6/Be multilayer coatings with 50 bilayers were applied to the concave replica gratings at Lawrence Livermore National Laboratory (LLNL) using the magnetron sputtering technique.[31]

It was found[5,7] that the calculated efficiencies of the Mo_4Ru_6/Be multilayer grating were very sensitive to variations in the groove profile. Small changes in the assumed groove shape, groove height, and facet angles resulted in significant changes in the calculated efficiencies. In this case, the average depth of modulation of the layers was scaled to achieve the best agreement with the experimental data at 11.375 nm wavelength where the efficiency was maximal. The depth of the profile of the replica grating substrate, as derived from the AFM measurements, is 8.5 nm.[5,19] During the process of coating the grating substrate with multiple layers to produce a multilayer grating, a smoothing of the groove profile takes place. As a result, the depth of modulation of the upper layers decreases. As the influence of diffraction by the upper layers on the absolute grating efficiency is higher than that of the lower layers, and because there was no information on the change of the profile modulation depth (and the profile deformation) from one layer to another, a model with an average (with respect to all layers) profile modulation depth was used. By scaling the initial groove profile of the replica grating, the groove profile was determined that resulted in the smallest least-squares difference between the calculated and measured efficiencies at a wavelength of 11.375 nm. The resulting depth was 6.5 nm, which means that the profile becomes appreciably smoother in the upper layers.

The microroughness was determined by integrating the power spectral density (PSD) function over the $4-40/\mu m$ spatial frequency range for the AFM data in the center of a grating before and after application of the MoRu/Be multilayer coating. The rms value of the microroughness derived from the PSD function before coating was 1.35 nm and included spikes that contributed significantly to the microroughness value.[7] The rms microroughness derived from the AFM image after coating, which included bump-type features,[7] was 0.93 nm in the integrated spatial frequency range. The Strehl factor[32] calculated for the same plane multilayer stack, the ratio of the reflectance maxima reduced by rough interfaces and the reflectance maxima obtained with perfect interfaces, was used to account for the layer interdiffusion and random microroughness of the Mo_4Ru_6/Be multilayer grating. The inferred microroughness, resulting in the best agreement between the peak values of the calculated and measured efficiency in the -2 order near 11.375 nm, was 1.03 nm. This is an intermediate value between the measured AFM data before and after coating. The random roughness topography of the grating was taken into account in the fit by applying the amplitude Debye-Waller factor[5] with the rms roughness of 1.03 nm for all interfaces. The periodical lateral-correlated component of the border roughness from the average AFM groove shape was included automatically by accounting for the real groove profile with a high degree of accuracy (210 points per period). An assumption about the absence of the vertical correlation between the border random roughness components was applied in this model.

The good agreement between the measured and calculated reflectances indicates the reliability of the optical constants derived from the tables of Henke *et al.* in this wavelength region.[4] For the purposes of this work, the updated refractive indices were derived from the compilations.[33] We also tried refractive index data from the handbook of Palik,[34] which are more suitable for longer wavelengths,[4,5] to find better agreement between the calculated and measured efficiencies in the 11.1–12.0 nm wavelength range.[19]
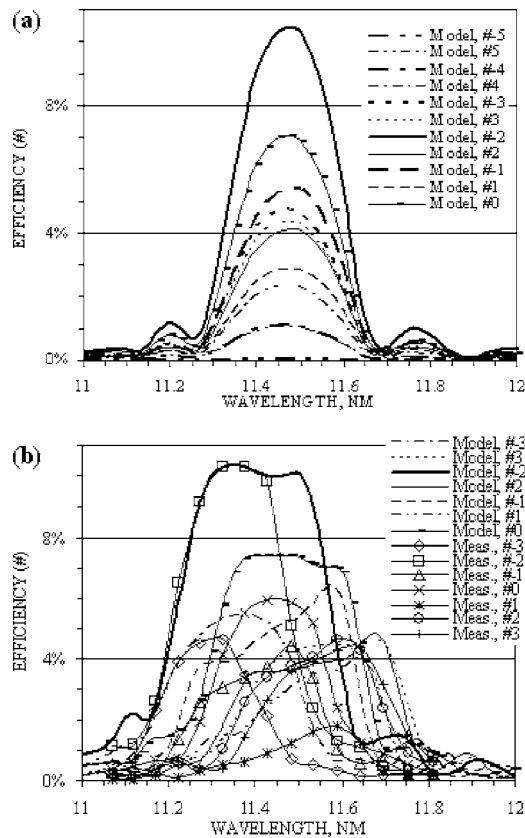
FIG. 7. The measured [(b), curves with markers], approximately calculated (a), and rigorously calculated [(b), curves without markers] efficiencies vs wavelength of the −3 to +3 orders of a 2400-groove/mm multilayer-coated grating with 50 MoRu/Be periods operating at an angle of incidence of 13.9°.

Figure 7 shows the measured and different calculated efficiencies in the diffraction orders of the Mo_4Ru_6/Be grating with 50 MoRu/Be periods. The measured inside and outside orders [Fig. 7(b)] are separated in wavelength while the efficiencies calculated[5,7] using Eq. (5) [Fig. 7(a)] are not. In contrast, the efficiencies calculated using the rigorous approach based on Eq. (41) are in good agreement with the measured data and with the phenomenological approach based on Eq. (11). As seen in Fig. 7, the calculated efficiency curves of some orders tend to be larger and wider than the respective measured efficiency curves. This may result substantially from scaling and averaging of the border profiles. When Eq. (5) is used, the computations execute much faster (by a few orders), owing to the implementation of approximate algorithms, but only the heights of order maxima are predicted well. To determine the spectral separation of the inside and outside orders and the exact shape and position of efficiency curves, rigorous electromagnetic theory for multilayer-coated gratings must be applied.

The time required to calculate one wavelength point for the MoRu/Be 103-border grating efficiency (with the energy balance error of ∼0.01%) was about 4 s for the approximate calculation model [Eq. (5)] and was about 10 min for the rigorous model when using an IBM® Think Pad with Intel® Pentium® M 1700 MHz processor, 1 Mbyte cache, 400 MHz bus clock, 512 Mbyte random access memory (RAM), and controlled by OS Windows® XP Pro. All mod-

eling in this section was performed for plane grating models, because the ratios of the grating sizes to radii of curvature and the incident beam sizes to grating sizes are small.

B. Investigation of the efficiency of a lamellar Mo/Si grating for Solar-B mission

Due to the high reliability and performance of multilayer Mo/Si coatings, they enjoy wide use in telescopes and normal-incidence spectrometers, both ground based and space borne. The EUV imaging spectrometer (EIS) developed for the Solar-B spacecraft[35] is an orbital instrument making use of a multilayer diffraction grating, and the Mo/Si coating was chosen and optimized for its optics.[8] The toroidal diffraction grating, 100 mm in diameter and with a nominal radius of 1.18 m, having 4200 grooves/mm and rectangular (trapezoidal) groove profile of nominal depth 58 Å, was fabricated holographically by Zeiss Lazer Optics GmbH, with subsequent ion etching of the fused silica substrate. Different Mo/Si coatings, optimized for operation in two narrow EUV wave bands (17–21 and 25–29 nm) containing many emission spectral lines (including those of the He II, Fe XII, and Fe XXIV ions), were deposited onto the two halves of the mirror and grating.

The measurements of the flight M2 mirror and FL1 grating were performed at the Naval Research Laboratory synchrotron beamline.[8] The efficiency was measured at 60 points of a square grid covering both parts of the working grating surface 90 mm in diameter. The efficiencies of the multilayer diffraction grating were measured at nine wavelengths with the radiation incident at an angle of 6.5° on the short-band side (from 17.1 to 22.0 nm) of the grating. Except for several extreme points at the edges of the working aperture, the efficiency was found to be quite uniform over the grating surface. The efficiencies of the FL1 grating measured at the central point of its short-wavelength side (gravitation center) are identified by markers in Fig. 8(b).

The theoretical diffraction efficiency was determined for unpolarized incidence radiation and parameters of the multilayer stack identical with the M2 mirror.[23] For the short-band half of the diffraction grating, these parameters are 20 Mo/Si layer pairs with a bilayer period D_{Bragg} =10.3 nm and a Mo thickness to bilayer period ratio Γ =0.37, 0.2 nm Si–Mo interface rms roughness, and 0.85 nm Mo–Si rms roughness. The Si protective capping layer is 2 nm thick. The trapezoidal groove profile based on AFM measurements has 6 nm depth, side slopes of 35°, and equal top and groove widths.[8] The boundary profile was assumed the same for all layers. The Strehl factor calculated for the same plane multilayer stack was used to account for the interdiffusion and random microroughness of the Mo/Si multilayer grating. The modeling was carried out using the refractive index data for Si and Mo taken from different sources.[4] There were no free parameters in the calculation.

Figure 8(b) indicates good agreement between the measured and rigorously calculated diffraction efficiencies of the FL1 grating in the ±1, 0, −3, and −5 orders in the entire working wavelength range. As pointed out above, while the physical model based on Eq. (5) does not yield wavelength
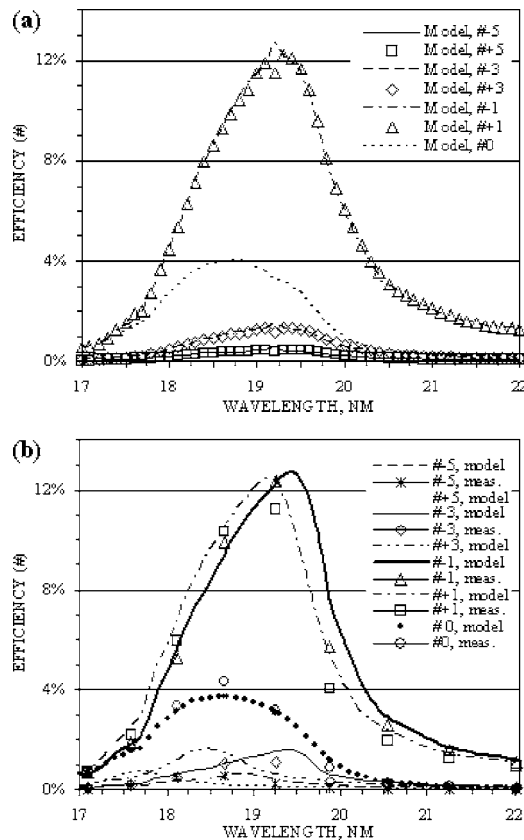
FIG. 8. The measured [(b), data markers], approximately calculated (a), and rigorously calculated [(b) curves] order efficiencies vs wavelength of the 4200-groove/mm multilayer-coated FL1 flight grating, with 20 Mo/Si periods on the short-band side of the EIS optics, operating at an angle of incidence of 6.5°.

separation of the inside and outside orders, this model is capable of accurately predicting for this particular groove profile the shape of the efficiency curves and the heights of their maxima [Fig. 8(a)]. The theoretical and experimental efficiencies of the FL1 grating, as well as the backup flight grating FL7, which were calculated with the approximate model based on Eq. (5), are presented in Refs. 4 and 8. The time required to calculate one wavelength point for the FL1 grating efficiency (with the energy balance error of ~0.01%) was about 1 s for the calculation based on Eq. (5) and about 1 min for the calculation based on Eq. (41) using the above mentioned computer.

C. Investigation of the efficiency of a blazed Mo/Y grating

One of the most intense emission lines in the shortest EUV spectral range is Fe XVIII at 9.392 nm. This line was observed in rotating cool stars and white dwarf systems and can be used, for example, to study magnetic fields. It is therefore of interest to develop high-resolution spectroscopic instruments based on high-efficiency diffraction gratings that operate in this wavelength region. Experimental measurements have demonstrated substantially high reflectance for Mo–Y multilayers and good stability.

An experimental and theoretical investigation of a normal-incidence Mo/Y multilayer-coated diffraction grat-

ing operating at a 9 nm wavelength was reported in Ref. 6. A replica of a concave holographic ion-etched blazed grating with 2400 grooves/mm was coated by a Mo/Y multilayer. The grating efficiency in the TM polarization was measured at the Lawrence Berkeley National Laboratory.[6] The Mo/Y multilayer coatings were applied to a planar witness substrate and the concave grating at LLNL. rms roughnesses were derived from the AFM measurements at LLNL.

The theoretical efficiencies of the Mo/Y multilayer diffraction grating were previously calculated using the model based on Eq. (5).[6] Here we report more accurate efficiency calculations of the Mo/Y grating at 8° incidence in the 9 nm wavelength region based on the rigorous multilayer MIM described in Sec. III. We used an averaged groove profile model as was done in the case of the MoRu/Be multilayer grating. The best fit was obtained with the master AFM-measured groove profile[5] scaled by a factor of 1.07 for all 203 boundaries. The real polygonal profile had 121 points.

Because of the space limitation and the deposition geometry, the grating and the flat witness substrate could not be coated simultaneously. Thus the multilayer interface parameters of the coating on the grating were inferred from fitting the measured and calculated efficiencies in the principal order. The measured peak efficiency in the −3 order was 2.7% at a wavelength of 8.79 nm. The best fit was obtained with D_{Bragg}=4.528 nm, Γ=0.445, N=100 bilayers, and the interface roughness of 0.96 nm, in good agreement with the designed parameters.[6] The Strehl factor calculated for the same plane multilayer stack was used to account for the interdiffusion and random microroughness of the Mo/Y multilayer grating. The interface roughness in the fit was assumed to be the same and noncorrelated for each interface, and the amplitude reduction by the Debye-Waller factor was applied. The rms roughness inferred from calculations, 0.96 nm, is near the average of the measured rms roughness before and after coating in the 4–40/μm spatial frequency range.[6]

Figure 9(a) shows the calculated spectral efficiencies of the Mo/Y 2400-groove/mm grating using the approximate model of Eq. (5). Again, Eq. (5) does not yield wavelength separation of the inside and outside orders and is not capable of accurately predicting the shape of the curves, although this model does determine well enough the values of the efficiency maxima. Figure 9(b) shows the measured and the calculated efficiencies, using the rigorous approach of Eq. (41), of the Mo/Y grating versus wavelength. There is excellent agreement between the measured and calculated efficiencies of this grating in the principal −3 order. The agreement for the high-efficiency −4 and −1 orders also is good. The agreement for the +1 and the low-efficiency orders is somewhat worse due to the unknown real border profiles for this particular Mo/Y 2400-groove/mm replica grating.

The time required to calculate one wavelength point for the Mo/Y 204-layer grating efficiency (with the energy balance error of ~0.01%) was about 1 s for the approximate calculation model of Eq. (5) and was about 18 min for the rigorous model of Eq. (41) using the above mentioned computer.
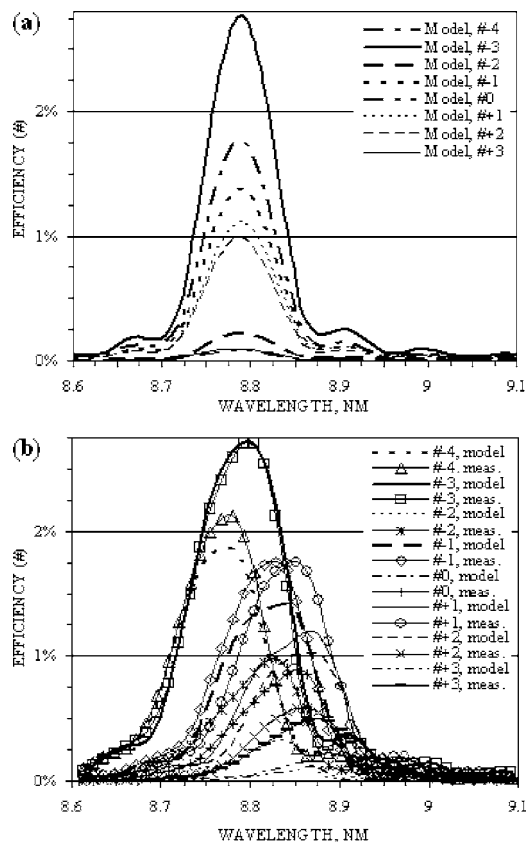
FIG. 9. The measured [(b), curves with markers], approximately calculated (a), and rigorously calculated [(b), curves without markers] efficiencies vs wavelength of the −4 to +3 orders of a multilayer-coated 2400-groove/mm grating with 100 Mo/Y periods operating at an angle of incidence of 8°.

V. SUMMARY AND CONCLUSION

The spectral separation of the inside and outside orders, which has been observed experimentally, was accounted for phenomenologically and by rigorous numerical modeling under the conditions of close to normal incidence of radiation on a multilayer-coated grating operating in the soft-x-ray-EUV spectral region. The reason for the observed substantial (a few angstroms or even nanometers) wavelength separation between the maxima of the inside and outside orders of a multilayer-coated grating operating in the short-wavelength range is related to the different angles of deviation of the respective orders. The wavelength separation occurs also with uncoated diffraction gratings but is not clearly pronounced because the efficiency is broad and slowly varying with wavelength.

The rigorous MIM, which is a variant of BIM and is designed for solving problems of diffraction from multilayer gratings in the soft-x-ray-EUV range with arbitrary layer thicknesses and boundary shapes, including boundaries with a real (for instance, AFM-measured) profile, is developed in a general form of the operator formalism. The MIM is a basis for the multilayer solver PCGRATE-S(X), which was chosen for the calculations described in this paper.

As follows from both the approximate and rigorous approaches, the spectral separation between the same number

inside and outside orders grows with increasing wavelength, angle of incidence, groove frequency, and diffraction order number.

To determine the shape and position of the efficiency curves in the soft-x-ray-EUV range, including bulk and multilayer-coated near-normal-incidence gratings with real boundary profiles, one should use codes based on rigorous electromagnetic theory for multilayer gratings, for instance, on the MIM.

For multilayer-coated gratings operating in diffraction orders near the Bragg peaks of the multilayer coating, the separation of the same number inside and outside orders in wavelength, although small, just as in the case of bulk gratings, is nevertheless quite significant and should be taken into account in the design and manufacture of high-resolution spectrometers. For example, spectrometers designed to accurately measure small wavelength shifts and spectral line shapes should account for the wavelength shift resulting from the wavelength-dependent order separation effect. This effect is a common property inherent in all bulk and multilayer diffraction gratings working in the soft-x-ray-EUV region under near normal incidence.

[1] J. F. Seely *et al.*, Appl. Opt. **36**, 8206 (1997).
[2] J. F. Seely, Proc. SPIE **4782**, 224 (2002).
[3] D. A. Content, P. Arsenovic, I. G. Kuznetsov, and T. Hadjimichael, Proc. SPIE **4485**, 405 (2001).
[4] J. F. Seely, L. I. Goray, D. L. Windt, Yu. A. Uspenskii, A. V. Vinogradov, and B. Kjornrattanawanich, Proc. SPIE **5538**, 43 (2004).
[5] L. I. Goray and J. F. Seely, Appl. Opt. **41**, 1434 (2002).
[6] B. Sae-Lao, S. Bajt, C. Montcalm, and J. F. Seely, Appl. Opt. **41**, 2394 (2002).
[7] J. F. Seely, C. Montcalm, S. Baker, and S. Bajt, Appl. Opt. **40**, 5565 (2001).
[8] J. F. Seely, C. M. Brown, D. L. Windt, S. Donguy, and B. Kjornrattanawanich, Appl. Opt. **43**, 1463 (2004).
[9] L. I. Goray, Nucl. Instrum. Methods Phys. Res. A **536**, 211 (2005).
[10] M. Neviere and F. Montiel, J. Opt. Soc. Am. A **13**, 811 (1996).
[11] L. I. Goray, Russ. Acad. Sci. Bull. Phys. **69**, 211 (2005).
[12] M. Neviere, J. Opt. Soc. Am. A **8**, 1468 (1991).
[13] B. Vidal, P. Vincent, P. Dhez, and M. Neviere, Proc. SPIE **563**, 142 (1985).
[14] D. Maystre, J. Opt. Soc. Am. **68**, 490 (1978).
[15] A. Pomp, J. Mod. Opt. **38**, 109 (1991).
[16] L. I. Goray, Proc. SPIE **5168**, 260 (2003).
[17] L. I. Goray and S. Yu. Sadov, in *Diffractive Optics and Micro-Optics*, OSA Trends in Optics and Photonics Vol. 75, edited by R. Magnusson (Optical Society of America, Washington, DC, 2002), p. 365.
[18] L. I. Goray, I. G. Kuznetsov, S. Yu. Sadov, and D. A. Content, J. Opt. Soc. Am. A **23**, 155 (2006).
[19] See website at www.pcgrate.com
[20] L. M. Brekhovskih, *Waves in Layered Media*, 2nd ed. (Academic, New York, 1980).
[21] E. G. Loewen and M. Neviere, Appl. Opt. **17**, 1087 (1978).
[22] E. G. Loewen, M. Neviere, and D. Maystre, J. Opt. Soc. Am. **68**, 496 (1978).
[23] L. I. Goray and J. F. Seely, Proc. SPIE **5900**, 81 (2005).
[24] *Electromagnetic Theory of Gratings*, edited by R. Petit (Springer, Berlin, 1980).
[25] M. C. Hutley, *Diffraction Gratings* (Academic, London, 1982).

[26]L. I. Goray and J. F. Seely, *Diffractive Optics 2005*, EOS Topical Meetings Digest Series, Warsaw, Poland, 3–7 September 2005, 83–922174–1–1p. 74, http://www.eurocongress.com.pl/do2005/DO_manuscript/index.html

[27]B. Kleemann, A. Mitreiter, and F. Wyrowski, J. Mod. Opt. **43**, 1323 (1996).

[28]D. Colton and R. Kress, *Integral Equation Methods in Scattering Theory* (Springer, Berlin, 1984).

[29]J. T. Beale and M.-C. Lai, SIAM (Soc. Ind. Appl. Math.) J. Numer. Anal. **38**, 1902 (2001).

[30]C. Schwab and W. L. Wendland, Math. Comput. **68**, 91 (1999).

[31]S. Bajt, J. Vac. Sci. Technol. A **18**, 557 (2000).

[32]D. G. Stearns, D. P. Gaines, D. W. Sweeney, and E. M. Gullikson, J. Appl. Phys. **84**, 1003 (1998).

[33]See website at http://www.cxro.lbl.gov/optical_constants/getdb2.html

[34]*Handbook of Optical Constant of Solids*, edited by E. Palik (Academic, New York, 1985), Vols. I and II.

[35]See website at http://solarb.msfc.nasa.gov/